Infrared extinction properties of nanostructured and conventional particles

Susana C. Pjesky and Ronaldo G. Maghirang

How to cite this manuscript

If you make reference to this version of the manuscript, use the following information:

Pjesky, S. C., & Maghirang, R. G. (2012). Infrared extinction properties of nanostructured and conventional particles. Retrieved from http://krex.ksu.edu

Published Version Information

Infrared Extinction Properties of Nanostructured and Conventional Particles

Susana C. Pjesky* and Ronaldo G. Maghirang**

_____

*Dr. Susana C. Pjesky (corresponding author), Bureau of Air, Kansas Department of Health and Environment, Topeka, KS USA 66612, Tel. no.: 785-296-1691, E-mail: spjesky@kdheks.gov

**Dr. Ronaldo G. Maghirang, Department of Biological & Agricultural Engineering, Kansas State University, Manhattan, KS USA 66506, Tel. no.: 785-532-2908, E-mail: rmaghir@ksu.edu

Abstract

Brass flakes and carbon-based particulates are effective obscurants in the infrared (IR) region of the electromagnetic spectrum; however, they are toxic and can cause respiratory problems and environmental concerns. There is a need to develop or identify nontoxic IR obscurants. This research was conducted to determine the potential of nanostructured particles as IR obscurants. Three commercial nanostructured particles were compared with two conventional particles and common obscurants. Experiments involved dispersing a known mass of particles into a particle chamber and measuring the IR transmission through the chamber with a Fourier transform infrared analyzer and the mass concentration with filter samplers. The size distribution of the aerosolized particles was also measured with an aerodynamic particle sizer spectrometer. From the measured data, the mean values of the mass extinction coefficient, σ_m, and volume extinction coefficient, σ_v, for the spectral bands of interest (i.e., 3 to 5 µm and 8 to 12 µm) were calculated. Results showed that ISO fine test dust, $NaHCO_3$ and NanoActive$^{\circledR}$ TiO_2 (for 3 to 5 µm) appeared to be the most promising alternatives to brass or graphite flakes. By manipulating the size and/or morphology of these particles, it might be possible to enhance their IR extinction performance.

Keywords: extinction coefficient, Fourier transform infrared (FTIR), infrared, nanostructured particles, obscurant

1 Introduction

Obscurants in the infrared (IR) region of the electromagnetic spectrum have played a major role in military operations because they provide protection of military personnel, equipment and installation from IR-seeking sensors of unfriendly forces [Singh et. al. (1994); Ladouceur et. al. (1997); Butler (1998); Shi et. al. (1998); Shi et. al. (2003)]. Obscurants that are effective in IR have received renewed interest because of the increasing threat of emerging IR sensors [Singh et. Al. (1994); Shi et. al. (2003); Farmer and Krist (1981); Farmer et. al. (1982); Appleyard and Davies (2004); Wang et. al. (2004)]. For obscurants to be considered effective, they must exhibit high extinction coefficients and, at the same time, not be harmful to human health and the environment. They also must be easy to deploy, readily available and cost-effective [Owrutsy et. al. (2000)].

The extinction coefficient, or extinction cross section, of an obscurant is a measure of its ability to attenuate the incident radiant energy at a certain wavelength [Shi et. al. (1998)]. It is expressed as either the mass extinction coefficient, σ_m, or volume extinction coefficient, σ_v [Owrutsy et. al. (2000)]. For military applications, the σ_v value of an obscurant is likely more important than the σ_m value because most deployment methods (e.g., grenade) are volume-limited rather than mass-limited [Owrutsy et. al. (2001)].

Extinction coefficients are typically expressed as averages over the spectral band of interest [Farmer (1991)]. In military applications, the wavebands of increasing importance are the 3- to 5-µm and 8- to 12-µm wavelengths in the mid-IR region. These ranges are the main "atmospheric windows," or regions in the electromagnetic spectrum, in which IR transmission is close to 100% regardless of the presence of atmospheric gases, including water vapor and carbon

dioxide (CO_2) [Jacobson (1999); Bailey et. al. (2002); Hutchison and Cracknell (2005)]. Milham (1976), however, observed IR absorption of CO_2 within the 4.1- to 4.4-μm wavelength range.

Many factors can influence the IR extinction properties of obscurants. In general, highly conducting materials (e.g., brass flakes and graphite flakes) are effective IR obscurants. Appleyard (2006) noted that, on the basis of theoretical analysis, the conductivity of the particles appeared to be the most important property that influences IR extinction performance. Salts, metal oxides and semiconductors generally have good IR absorption properties because of their moderately strong molecular vibrations in the IR region [Owrutsky et. al. (2001); Stuart (2004)]. Other factors that affect extinction properties include chemical composition, size distribution, concentration and morphology [Ladouceur et. al. (1997); Shi et. al. (1998); Widmann et. al. (2005)]. Morphology is particularly important because it influences the coagulation process and removal of particles from the air [Colbeck et. al. (1997)]. Structures such as thin disc flakes and thin fibers have exhibited high extinction coefficients [Appleyard and Davies (2004); Appleyard (2006)]. The molecular structure of the material, primary particle size and structure of the aggregate also affect the effectiveness of obscurants [Shi et. al. (1998); Dobbins et. al. (1994)].

Although brass exhibits favorable obscuration properties, it is highly toxic (rated 9 by the U.S. Environmental Protection Agency (EPA) on a scale of 0-9) and environmentally detrimental [Owrutsky et. al. (2000); Haley and Kurnas (1993)]. Graphite has a much lower toxicity (EPA toxicity rating of 4) and less environmental effect than brass [Owrutsky et. al. (2000); Haley and Kurnas (1993)]; however, its packing density is much lower than that of brass [Ladouceur et. al. (1997)]. Carbon black, another carbonaceous material like graphite, has been identified by Owrutsky et. al. (2001) as one of the best obscurants. Like graphite, however, carbon black has a much lower packing density than brass.

There is a need to develop or identify nontoxic IR obscurants. This research was conducted to evaluate the extinction coefficients of nanostructured particles in the mid-IR range. The σ_m and σ_v values of the nanostructured particles were determined and compared with those of conventional particles and common obscurants.

2 Materials and Methods

2.1 Experimental apparatus

The experimental apparatus had three major components: FTIR spectrometer (Nicolet Model 6700), particle chamber and powder disperser. The FTIR spectrometer was configured to provide mid-IR radiation (i.e., 1.35- to 25-µm wavelength) and was calibrated using monodisperse polystyrene spheres. The OMNIC™ software (Thermo Fisher Scientific, Inc., Waltham, MA) was used to acquire, process and analyze the spectral data [Thermo Electron Corporation (2006)]. The particle chamber (Figure 1) was set up on top of the sampling compartment of the FTIR spectrometer. The chamber was 40.6 cm wide, 16.5 cm thick, and 63.5 cm high. Near the bottom on each side of the chamber were two holes with PVC pipes (3.81 cm in diameter and 2.54 cm long) for the passage of the IR beam produced by the FTIR spectrometer. Two filter samplers were placed directly above the two PVC pipes for time-averaged measurement of particle mass concentration. The samplers consisted of 37-mm glass fiber filters on plastic cassette holders. An aerodynamic particle sizer® (APS) spectrometer (Model 3321, TSI Inc, Shoreview, MN.) was used to monitor the aerodynamic diameter and number concentration of the airborne particles. The chamber was also equipped with a small fan for initial mixing of particles and sliding doors to protect the KBr optical windows of the spectrometer.

A known mass (approximately 3 g) of particles was placed inside the powder disperser, which was connected to a compressed nitrogen gas tank (tank pressure gauge was set at 30 psig) through a hose and a nozzle. To disperse the particles into the chamber, the nozzle was manually pressed for up to approximately < 2 seconds until most of the particles were dispersed.

2.2 Particulate obscurants

Three types of particles were considered in the study: nanostructured metal oxide particles (i.e., NanoActive[®] MgO plus, NanoActive[®] MgO and NanoActive[®] TiO_2) (NanoScale Corp., Manhattan, KS), conventional particles (i.e., $NaHCO_3$ and ISO fine test dust) and reference obscurants (i.e., brass flakes, graphite flakes and carbon black). Figures 2-4 show scanning electron microscope images of the particles. The brass flakes (Premior 505, Wolsteinholme Inter'l. Inc., West Chicago, IL), graphite flakes (Asbury Graphite Mills, Inc., Asbury, NJ) and carbon black (Asbury Graphite Mills, Inc., Asbury, NJ) were chosen as reference particles because they are the most commonly studied obscurants [Owrutsky et. al. (2000); Owrutsky et. al. (2001)]. Table 1 summarizes properties of the particles such as their surface area and chemical composition. Brass is one of the best predicted attenuators of IR radiation [Appleyard (2007)] and the obscurant most commonly used by the military. The NanoActive® metal oxide powders were selected because of their unique morphology, large surface areas and relatively nontoxic nature. Also, TiO_2 is a semiconductor, is expected to have good values of extinction coefficient, and has an EPA toxicity rating of 0 [Owrutsky et. al. (2000); Haley and Kurnas (1993)]. ISO fine test dust was selected for its good conductivity and flaky structure; $NaHCO_3$ was selected because it is relatively nontoxic and a salt.

2.3 Experimental procedure

The particle chamber (Figure 1) was first conditioned by flushing it with dry compressed air for at least 30 min to remove or reduce any water vapor inside the chamber. A background spectrum (i.e., without the obscurant) was collected before dispersion of the particles into the chamber. Then, the sliding door in front of the KBr optical window of the FTIR spectrometer was closed to protect the KBr optics from particles that might stick into it upon dispersion of particles. The mixing fan inside the chamber was turned on, and particles were dispersed into the chamber by manually pressing the nozzle of the powder disperser. Once particles were dispersed, the fan was turned off and the sliding doors were opened to let the IR beam pass through the two KBr windows.

The sample spectrum was obtained with OMNIC™ software. The software was also configured such that the sample spectrum was divided by the background spectrum (called "ratioing") to account for the spectral characteristics of the chamber and the instrument (i.e., IR absorption due to any atmospheric water vapor and CO_2) [Thermo Electron Corporation (2006)].

After the first sample spectrum was obtained, the sampling pump of the filter samplers was started and operated for 1 min at a sampling rate of 2 L/min. After particle sampling, another sample spectrum was obtained. The APS spectrometer was started from the time the first sample spectrum was obtained.

The IR transmittance (T^*) values measured by the FTIR spectrometer were converted to absorbance (A) values using the OMNIC software [Thermo Electron Corporation (2006)]. These A values and the particle mass concentration, C_m, obtained from the filter samplers were then used to calculate the σ_m value on the basis of Beer's law, which relates the optical measurement to the C_m of the obscurant [Smith (1996)]:

$$\sigma_{m_{(\lambda)}} = \frac{2.303A_{(\lambda)}}{C_m L}$$

where λ is wavelength and L is the path length.

The calculated σ_m values "after dispersion" (i.e., t = 1 min after dispersion) and "after particle sampling" (i.e., t = 3 min after dispersion) were averaged to get the "mean σ_m" value. This value was considered equivalent to time 2 min after dispersion when the C_m and aerodynamic diameter were measured simultaneously. The "mean σ_m" values for the 3- to 5-µm and for the 8- to 12-µm wavebands were calculated. The σ_v value was obtained by multiplying the σ_m value and the tap density, which was measured in accordance with ASTM Standard B 527-93 [ASTM Standards (2006)].

In addition, the overall mean σ_m and σ_v values for each replicate were obtained by averaging the "mean σ_m" and "mean σ_v" values for the 3-to 5-µm and 8- to 12-µm wavelengths.

Data were analyzed statistically using SAS (version 9.1, SAS Institute Inc., Cary, NC). The PROC GLM procedure and correlation analysis were used to determine the effect of the particles' type, concentration and diameter on extinction coefficients. The means were also compared at $\alpha = 0.05$ using the Tukey's Studentized Range and Scheffe's Test for equal and unequal number of replications.

3 Results and Discussion

3.1 Mass extinction coefficients

The reference particles (i.e., brass flakes, graphite flakes and carbon black) showed nearly constant values of σ_m throughout the 3- to 12-µm wavelength range (Figure 5), a trend similar to those observed in previous studies [Owrutsky et. al. (2001); Appleyard (2006); Wetmore and Ayres (2000)]. In contrast, the σ_m values of the nanostructured and conventional

particles varied considerably with wavelength. These trends were similar to those of many military obscurants, including red phosphorus and fog oil [Farmer (1991); Milham (1976)]. Within the 4.1- to 4.4-μm wavelength range, the IR absorption of CO_2 can be observed [Milham (1976)]. In the wavelength range between 5 and 8 μm, the collective absorption of water vapor, CO_2 and other gases can be observed as indicated by fluctuations in σ_m with wavelength [Bailey et. al. (2002)].

Table 2 summarizes the mean values of the band-averaged σ_m, mass dispersed and mass concentrations of the particles. The reference particles had the greatest band-averaged σ_m values. The mean σ_m values for the 3- to 5-μm waveband for brass flakes, graphite flakes and carbon black were 1.44 (s.d. = 0.34), 3.03 (s.d. = 0.40) and 1.89 (s.d. = 0.31) m^2/g, respectively; values for the 8- to 12-μm waveband were 1.62 (s.d. = 0.37), 3.31 (s.d. = 0.41) and 1.66 (s.d. = 0.45) m^2/g, respectively. Wetmore and Ayres (2000) cited a σ_m value of 2 m^2/g for both the 3- to 5-μm and 8- to 12-μm wavebands for graphite flakes. Owrutsky et al. [Owrutsky et. al. (2000); Owrutsky et. al. (2001)] reported smaller σ_m values for brass flakes (0.34 m^2/g and 0.33 m^2/g for 3- to 5-μm and 8- to 12-μm waveband, respectively), graphite flakes (0.74 m^2/g and 0.73 m^2/g for 3- to 5-μm and 8- to 12-μm waveband, respectively) and carbon black (0.83 m^2/g and 0.62 m^2/g for 3- to 5-μm and 8- to 12-μm waveband, respectively). Differences between the measured values in this study and to other published values could be due to differences in the properties of particles used (i.e., mean particle size, shape and morphology) and measurement methods. For example, Owrutsky et. al. (2000) used graphite particles with nominal particle size of 2 μm while in this study graphite flakes with geometric mean diameter (GMD) of 3.87μm were used. Also, Owrutsky et. al. (2000) used a different experimental set-up such that the particles were

entrained in a continuously flowing gas stream while being measured whereas in this study particles were dispersed into the chamber using 30 psig of nitrogen gas.

Of the nanostructured and conventional particles considered, NanoActive[®] TiO_2 had the greatest mean σ_m value for the 3- to 5-μm waveband (Table 2). The mean σ_m value of NanoActive® TiO_2 in the 3- to 5-μm range (1.10 m^2/g, s.d. = 0.23), however, did not significantly differ ($\alpha = 0.05$) from those of the other nanostructured and conventional particles. As mentioned earlier, TiO_2 is a semiconductor and was expected to exhibit good extinction performance. For the 8- to 12-μm wavelength region, the ISO fine test dust had the greatest mean σ_m value (0.75 m^2/g, s.d. = 0.03); however, the mean σ_m value was not significantly different from those of the other particles. ISO fine test dust consists of several semiconductive elements such as silicates, aluminum and iron [Vlasenko et. al. (2005)] and also has a flaky structure.

3.2 Volume extinction coefficients

Table 3 summarizes the mean values of the band-averaged σ_v and tap densities of the particles. $NaHCO_3$ (1.39 g/cc, s.d. = 0.001), ISO fine test dust (1.22 g/cc, s.d. = 0.00) and brass flakes (1.05 g/cc, s.d. = 0.006) had the largest tap densities.

The reference particles showed near constant σ_v values; however, both graphite flakes and carbon black showed marked decreases in σ_v values ($\approx$75 to 78% decrease compared with their corresponding σ_m values) because of their low tap densities (Figure 6; Table 3). The brass flakes sample, on the other hand, maintained its extinction coefficient value because of its high tap density (1.05 g/cc).

For the 3- to 5-μm wavelength region, brass flakes had the highest σ_v value (1.5 m^2/cc, s.d. = 0.36) (Table 3), followed by the two conventional particles, $NaHCO_3$ (1.01 m^2/cc, s.d. =

10

0.16) and ISO fine test dust (0.87 m^2/cc, s.d. = 0.02), and NanoActive® TiO_2 (0.88 m^2/cc, s.d. = 0.19). Brass flakes also had the highest value (1.69 m^2/cc, s.d. = 0.40) for the 8- to 12-μm waveband. The next highest σ_v values were those of ISO fine test dust (0.91 m^2/cc, s.d. = 0.04), $NaHCO_3$ (0.89 m^2/cc, s.d. = 0.13) and graphite flakes (0.82 m^2/cc, s.d. = 0.10). The nanostructured MgO particles had the smallest σ_v values for both wavebands. Brass flakes had the greatest overall mean σ_v values (1.64 m^2/cc, 0.39), followed by $NaHCO_3$ (0.93 m^2/cc, 0.12), ISO fine test dust (0.91 m^2/cc, 0.03) and graphite flakes (0.80 m^2/cc, 0.10).

3.3 Effect of particle size distribution and concentration

Figure 7 shows the particle size distributions at time 1 min after dispersion. The values of geometric mean diameter (GMD), geometric standard deviation (GSD), mass concentration and number concentration are shown in Table 4. NanoActive® MgO plus had the highest GMD value of 8.32 μm (s.d. = 0.25). NanoActive® MgO had a wider size distribution (GSD=2.61, s.d. = 0.12) and the highest particle number concentration (403,333 particles/cc, s.d. = 13051). $NaHCO_3$ had the highest mass concentration (1,777 mg/m^3, s.d. = 298). Statistical analysis showed that the GMD, GSD and particle concentration did not have any significant effect on values of σ_m and σ_v.

Results in this study generally agree with published data [Appleyard and Davies (2004); Owrutsky et. al. (2001); Appleyard (2006)]. Appleyard and Davies (2004) concluded that high-aspect ratio, highly conducting small particles (i.e., aluminum and brass) are excellent IR obscurants. In this study, brass flakes had the largest σ_v value and the third largest σ_m value (Table 4). The brass flakes sample in this study had 69 to 91% copper and 29.5 to 7.5% zinc, which have electrical conductivity values of 100% International Annealed Copper Standard (IACS) and 28% IACS, respectively. Aside from the high conductivity of brass flakes, the flake-

like structure (≈ 5 µm major diameter) with clumps of threadlike particles (thickness < 500 nm) appears to be important. These results agree with the theoretical results of Appleyard and Davies (2004) and Appleyard (2006) that structures such as thin disk flakes and thin fibers have high extinction coefficients.

In this study, graphite flakes had the greatest overall σ_m value (3.22 m^2/g), followed by carbon black (1.72 m^2/g) and brass flakes (1.57 m^2/g) (Table 4). Graphite and carbon black are composed of more than 99% carbon and have moderate to strong molecular vibrations in the IR region [Owrutsky et. al. (2001); Sturat (2004)] but differ in morphology (Figures 4b-4c) . Graphite has a flaky structure, whereas carbon black has a very small primary particle size (35 nm) and particles that seem to aggregate. Owrutsky et al. (2001) measured the σ_m and σ_v values for several powders being considered as new obscurant candidate materials including salts, semiconductors and oxides. They reported that graphite had the largest σ_m value but a lower σ_v value than brass, similar to the findings in this study.

NaHCO$_3$ and ISO fine test dust have similar morphology—smaller, flat particles that are irregularly stacked on each other (Figure 3a-3b). The overall σ_m values of NaHCO$_3$ and ISO fine test dust were 0.67 m^2/g (s.d.=0.08) and 0.74 m^2/g (s.d.=0.03), respectively, which are smaller than those of the reference particles (Table 4). NaHCO$_3$ and ISO fine test dust had larger packing densities and larger σ_v values than graphite and carbon black. On the basis of σ_v values, ISO fine test dust and NaHCO$_3$ appear to be the most promising alternatives to brass flakes. By manipulating the size and/or morphology of these two particles, it might be possible to enhance their IR extinction performance.

In general, the NanoActive® metal oxide particles had relatively poor IR extinction performance (Table 4). And because of their relatively small packing density (< 0.8 g/cm^3), the

numerical values of σ_v were even smaller than those of σ_m. This agrees with the experimental results of Owrutsky et al. (2001); measured extinction coefficients of metal oxide particles, including titanium oxide, aluminum oxide and manganese oxide were relatively small. It should be noted, however, that NanoActive® TiO_2 had a relatively high σ_m value in the 3- to 5-µm waveband. Appleyard and Davies (2004) indicated that particles of insulating and semiconducting materials that are ionic and partially ionic possess extinction spectra that are particle size dependent but relatively insensitive to particle geometry.

4 Conclusions

This research was conducted to identify effective obscurants in the mid-IR range and compare them with common military IR obscurants such as brass flakes, graphite flakes and carbon black. The following conclusions were drawn from this research:

(1)   Graphite flakes had the greatest overall mean mass extinction coefficient (3.22 m^2/g, s.d. = 0.40), followed by carbon black (1.72 m^2/g, 0.41), brass flakes (1.57 m^2/g, 0.38) and ISO fine test dust (0.74 m^2/g, 0.03). Brass flakes had the greatest overall mean volume extinction coefficient (1.64 m^2/cc, 0.39), followed by $NaHCO_3$ (0.93 m^2/cc, 0.12), ISO fine test dust (0.91 m^2/cc, 0.03) and graphite flakes (0.80 m^2/cc, 0.10). The geometric mean diameter, geometric standard deviation and particle concentration did not have any significant effects on the values of σ_m and σ_v. It appears that high-aspect ratio (i.e., thin disk flakes and thin fibers) and high conductivity are the main factors contributing to high IR extinction coefficients;

(2)   The extinction coefficients of the NanoActive® materials were generally significantly smaller than those of the reference and conventional particles. NanoActive® TiO_2 did have a relatively high σ_m value in the 3- to 5-µm waveband; and

(3)   On the basis of the values of volume extinction coefficient for specific wavebands, the

following materials appeared to be the most promising alternatives to brass flakes: ISO

fine test dust and $NaHCO_3$ (for both the 3-5 and 8-12 μm wavebands) and NanoActive™

TiO_2 (for 3 to 5 μm waveband). Note, however, the extinction coefficients of these

materials varied considerably with wavelength, while that of brass flakes did not vary

much with wavelength.

Further research is needed to investigate the effectiveness of these materials field

conditions. In addition, effects of surface chemistry of the materials on IR extinction

performance require further investigation.

5 Acknowledgements

6 Nomenclature

Symbols

L   m   Path length

C_m $mg·m^{-3}$ Particle mass concentration

σ_m $m^2·g^{-1}$ Mass extinction coefficient

σ_v $m^2·cc^{-1}$ Volume extinction coefficient

14

| T* | | Transmittance |
| λ | μm | Wavelength |

Abbreviations

APS	Aerodynamic Particle Sizer
EPA	Environmental Protection Agency
FTIR	Fourier Transform Infrared
GMD	Geometric Mean Diameter
GSD	Geometric Standard Deviation
IACS	International Annealed Copper Standard
IR	Infrared

7 References

Appleyard, P. G. 2006. Infrared Extinction Performance of High Aspect Ratio Carbon Nanoparticles. *J. Optic. Pure Appl. Optic. 8*, 101-113.

Appleyard, P. G. 2007. Modelled Infrared Extinction and Attenuation Performance of Atmospherically Disseminated High Aspect Ratio Metal Nanoparticles. *J. Optic. Pure Appl. Optic.*, *9*, 278-300.

Appleyard, P.G. and N. Davies. 2004. Calculation and Measurement of Infrared Mass Extinction Coefficients of Selected Ionic and Partially Ionic Insulators and Semiconductors: A guide for Infrared Obscuration Applications. *Opt. Eng.*, *43*, 376-386.

Appleyard, P. G. and N. Davies, 2004. Modelling Infrared Extinction of High Aspect Ratio, Highly Conducting Small Particles. *J. Optic. Pure Appl Optic.*, *6*, 977-990.

ASTM Standards. 2006. B 527-93: Standard Test Method for Determination of Tap Density of Metallic Powders and Compounds. Philadelphia, PA: ASTM.

Bailey, R. A., H. M. Clark, S. Krause, J. P. Ferris, and R. L. Strong. 2002. *Chemistry of the Environment.* 2nd ed. New York, NY: Elsevier.

Butler, B. A. 1998. *Smoke and Obscurant Operations in Adjoint Environments*. Unpublished Thesis. Maxwell Air Force Base, AL.

Colbeck, I., B. Atkinson, and Y. Johar. 1997. The Morphology and Optical Properties of Soot Produced by Different Fuels. *J. Aerosol Sci.*, *28*, 715-723.

Dobbins, R. A., G. W. Mulholland, and N. P. Bryner. 1994. Comparison of a Fractal Smoke Optics Model with Light Extinction Measurements. *Atmos. Environ.*, *28*,:889-897.

Farmer, W. M. 1991. Prediction of Broad-Band Attenuation Computed using Band-Averaged Mass Extinction Coefficients and Band-Averaged Transmittance. *Opt. Eng.*, *30*, 1255-1261.

Farmer, W. M. and K. L. Krist. 1981. Comparison of Methods Used to Determine the Mass Extinction Coefficient for Phosphorous Smokes. *Proc. Soc. Photo Opt.l Instrum. Eng.*, *305*, 7-16.

Farmer, W. M., F. A. Schwartz, R. D. Morris, M. A. Binkley, and L. M. Boyd. 1982. Optical Characteristics at 3.4-µm Wavelength of Munition-Produced Phosphorus Smoke as a Function of Relative Humidity. *Aerosol Sci. Tech.*, *1*, 409-425.

Haley, M. V. and C. W. Kurnas. 1993. Toxicity and Fate Comparison Between Several Brass and Titanium Oxide Powders. ERDEC-TR-094, Edgewood, MD: Edgewood Research and Development and Engineering Center.

Hutchison, K. D. and A. P. Cracknell. 2005. *Visible Infrared Imager Radiometer Suite: A New Operational Cloud Imager.* New York, NY: Taylor & Francis.

Jacobson, M. Z. 1999. *Fundamentals of Atmospheric Modeling.* UK: Cambridge University Press.

Ladouceur, H. D., A. P. Baronavski, and H. H. Nelson. 1997. *Obscurants for Infrared Countermeasures*. Washington, DC: Naval Research Lab.

Milham, M. 1976. A Catalog of Optical Extinction Data for Various Aerosols/Smokes. ED-8P-770022-85. Edgewood, MD: Edgewood Arsenal, Aberdeen Proving Ground.

Owrutsky, J. C., H. H. Nelson, H. D. Ladouceur, and A. P. Baronavski. 2000. *Obscurants for Infrared Countermeasures II*. Washington, DC: Naval Research Lab.

Owrutsky, J. C., D. A. Steinhurst, H. D. Ladouceur, H. H. Nelson, and A. P. Baronavski. 2001. *Obscurants for Infrared Countermeasures III.* Washington, DC: Naval Research Lab.

Shi, J. M., L. L. Chen, Y. S. Ling, and Y. Lu. 1998. Infrared Extinction of Artificial Aerosols and the Effects of Size Distributions. Int. J. Infrared Millimet. Waves., 19, 1671-1679.

Shi, J.M., J. Y. Wang, B. Xu, J. C. Wang, and Z. C. Yuan. 2003. Calculation and Optimization of the Effective Extinction Cross Section of the Spherical Cold Obscuring Smoke. *Int. J. Infrared Millimet. Waves.*, *24*, 2007-2013.

Singh, A., S. G. Avachat, and H. Singh. 1994. Infrared Screening Smokes - A Review. *J. Sci. Ind. Res.*, *53*, 667-673.

Smith, B. C. 1996. *Fundamentals of Fourier Transform Infrared Spectroscopy*. Baton Roca, FL: CRC Press.

Stuart, B. 2004. *Infrared Spectroscopy: Fundamentals and Applications*. Chichester, England: J. Wiley and Sons, Ltd.

Thermo Electron Corporation. 2006. Nicolet^{TM} FT-IR User's Guide. Madison, WI.

Wang, J. Y., J. M. Shi, B. Xu, J. C. Wang, and Z. C. Yuan. 2004. Calculation of Overall Effective Extinction Cross Section of Several Cold Smoke Infrared Ammunitions. *Defense Sci. J., 54*, 329-334.

Wetmore, A. and S. D. Ayres. 2000. Combined Obscuration Model for Battlefield Induced Contaminants. ARL-TR-1831-2 Vol. 2. Adelphi, MD: Army Research Laboratory.

Widmann, J.F., J. C. Yang, T. J. Smith, S. L. Manzello, and G. W. Mulholland. 2004. Measurement of the Optical Extinction Coefficients of Post-Flame Soot in the Infrared. *Combust. Flame. 134*, 119-129.

Vlasenko, A., S. Sjogren, E. Weingartner, H.W. Gaggeler, and M. Ammann. 2005. Generation of Submicron Arizona Dust Aerosol: Chemical and Hygroscopic Properties. *Aerosol Sci. Tech.*, *39*, 452-460.

Table 1: Physical and chemical properties of the particles.

Particle	Appearance/color	Surface area (m^2/g)	Major chemical composition (Percent by weight)	True density[f] (g/cm^3)
NanoActive® particles				
NanoActive® MgO plus[a]	white powder	≥ 600	99.62% Mg	2.46
NanoActive® MgO[a]	white powder	≥ 230	95% Mg	3.44
NanoActive® TiO$_2$[a]	white powder	≥ 500	99.99% Ti	3.64
Conventional particles				
NaHCO$_3$ (siliconized)[b]	white powder	-	93% NaHCO$_3$	2.27
ISO Fine test dust[c]	reddish brown powder	-	68-76% SiO$_2$ 10-15% Al$_2$O$_3$	2.76
Reference obscurants				
Brass flakes[d]	brass/bronze powder	1.2	69-91% Copper 7.5-29.5% Zinc	6.54
Graphite flakes[e]	dark gray powder	17	99.17% carbon	2.03
Carbon black[e]	black powder	36	99.73% carbon	1.80

[a]Source: NanoScale Materials, Inc., Manhattan, KS

[b]Source: Amerex Corp., Trussville, AL

[c]Source: PTI Powder Technolgy, Inc., Burnville, MN

[d]Source: Wolstenholme International Inc., Chicago, IL

[e]Source: Asbury Graphite Mills, Inc., Asbury, NJ

[f]Measured using multipycnometer

Table 2: Band-averaged mass extinction coefficients, mass dispersed and mass concentrations of particles. Each value represents the mean of three replicates.

| Particle | Mass extinction coefficient, m^2/g | | | | | | Mass dispersed, g | | Mass concentration, g/m^3 | |
| | 3-5 μm | | 8-12 μm | | Overall | | | | | |
	Mean[a]	s.d.	Mean[a]	s.d.	Mean[a]	s.d.	Mean	s.d.	Mean	s.d.
NanoActive® particles										
NanoActive® MgO plus	0.50 (d)	0.05	0.15 (c)	0.01	0.23 (d)	0.01	3.04 (a)	0.01	1.7 (abc)	0.27
NanoActive® MgO	0.67 (cd)	0.02	0.10 (c)	0.10	0.24 (d)	0.02	2.39 (a)	0.25	0.96 (bc)	0.13
NanoActive® TiO_2	1.10 (bcd)	0.23	0.23 (c)	0.05	0.43 (d)	0.09	2.50 (a)	0.41	1.6 (abc)	0.41
Conventional particles										
$NaHCO_3$	0.76 (cd)	0.09	0.64 (c)	0.06	0.67 (d)	0.08	2.85 (a)	0.18	1.56 (abc)	0.42
ISO Fine test dust	0.71 (cd)	0.01	0.75 (bc)	0.03	0.74 (cd)	0.03	2.50 (a)	0.05	0.76 (bc)	0.08
Reference obscurants										
Brass flakes	1.44 (bc)	0.34	1.62 (b)	0.37	1.57 (bc)	0.38	3.01 (a)	0.00	2.62 (a)	0.26
Graphite flakes	3.03 (a)	0.40	3.31 (a)	0.41	3.22 (a)	0.40	2.99 (a)	0.03	2.15 (ab)	0.38
Carbon black	1.89 (b)	0.31	1.66 (b)	0.45	1.72 (b)	0.41	2.85 (a)	0.08	2.04 (ab)	0.45

[a] Column means followed by the same letter are not significantly different at the 5% level.

Table 3: Band-averaged volume extinction coefficients and tap densities of particles. Each value represents the mean of three replicates.

Particle	Volume extinction coefficient, m^2/cc						Tap density, g/cc	
	3-5 μm		8-12 μm		Overall			
	Mean[a]	s.d.	Mean[a]	s.d.	Mean[a]	s.d.	Mean[a]	s.d.
NanoActive® particles								
NanoActive® MgO plus	0.33 (cd)	0.04	0.10 (c)	0.01	0.16 (d)	0.01	0.65 (f)	0.00
NanoActive® MgO	0.47 (cd)	0.02	0.07 (c)	0.01	0.17 (d)	0.01	0.71 (e)	0.00
NanoActive® TiO$_2$	0.88 (bc)	0.19	0.18 (c)	0.04	0.35 (d)	0.07	0.80 (d)	0.00
Conventional particles								
NaHCO$_3$	1.01 (ab)	0.16	0.89 (b)	0.13	0.93 (b)	0.12	1.39 (a)	0.00
ISO Fine test dust	0.87 (bc)	0.02	0.91 (b)	0.04	0.91 (b)	0.03	1.22 (b)	0.00
Reference obscurants								
Brass flakes	1.50 (a)	0.360	1.69 (a)	0.40	1.64 (a)	0.39	1.05 (c)	0.01
Graphite flakes	0.75 (bc)	0.100	0.82 (b)	0.10	0.80 (bc)	0.10	0.25 (g)	0.00
Carbon black	0.42 (cd)	0.070	0.37 (bc)	0.10	0.38 (bcd)	0.09	0.22 (h)	0.00

[a] Column means followed by the same letter are not significantly different at the 5% level.

Table 4: Overall mean values and standard deviations of extinction coefficients, geometric mean diameter (GMD) , geometric standard deviation (GSD), and mass and number concentrations of the particles at time 2 min after dispersion. Each value represents the mean of three replicates.

Particles	Overall σ_m		Overall σ_v		GMD, µm		GSD		Mass Conc., mg/m³		Number Conc., #/cc	
	Mean[a]	s.d.	Mean[a]	s.d.	Mean[a]	s.d.	Mean[a]	s.d.	Mean[a]	s.d.	Mean[a]	s.d.
NanoActive® particles												
NanoActive® MgO plus	**0.23 (d)**	0.01	**0.16 (d)**	0.01	**8.32 (a)**	0.25	**1.65 (c)**	0.05	**1453 (ab)**	185	**123667 (ab)**	19502
NanoActive® MgO	**0.24 (d)**	0.02	**0.17 (d)**	0.01	**4.86 (cd)**	0.49	**2.61 (a)**	0.12	**423 (bc)**	108	**403333 (a)**	13051
NanoActive® TiO$_2$	**0.43 (d)**	0.09	**0.35 (d)**	0.07	**4.87 (cd)**	0.68	**1.84 (bc)**	0.01	**639 (bc)**	304	**229667 (ab)**	24502
Conventional particles												
NaHCO$_3$	**0.67 (d)**	0.08	**0.93 (b)**	0.12	**5.89 (bc)**	0.13	**1.74 (c)**	0.03	**1777 (a)**	298	**234667 (ab)**	25697
ISO Fine test dust	**0.74 (cd)**	0.03	**0.91 (b)**	0.03	**3.73 (cd)**	0.58	**1.87 (bc)**	0.01	**403 (bc)**	56	**137000 (ab)**	21656
Reference obscurants												
Brass flakes	**1.57 (bc)**	0.38	**1.64 (a)**	0.39	**3.23 (d)**	0.28	**1.63 (c)**	0.05	**140 (c)**	74	**58067 (b)**	11686
Graphite flakes	**3.22 (a)**	0.40	**0.80 (bc)**	0.10	**3.87 (cd)**	0.35	**1.92 (bc)**	0.06	**810 (abc)**	669	**190367 (ab)**	158214
Carbon black	**1.72 (b)**	0.41	**0.38 (bcd)**	0.09	**7.47 (ab)**	0.73	**2.11 (b)**	0.14	**521 (bc)**	60	**354000 (ab)**	149171

[a] Column means followed by the same letter are not significantly different at the 5% level.

Chamber extension for gas
pressure release

Compressed
nitrogen

**Particle
Disperser**

**APS sampling
tube**

**Filter
Samplers**

**IR
detector**

**IR
source**

Mixing Fan

16.5 cm

40.6 cm
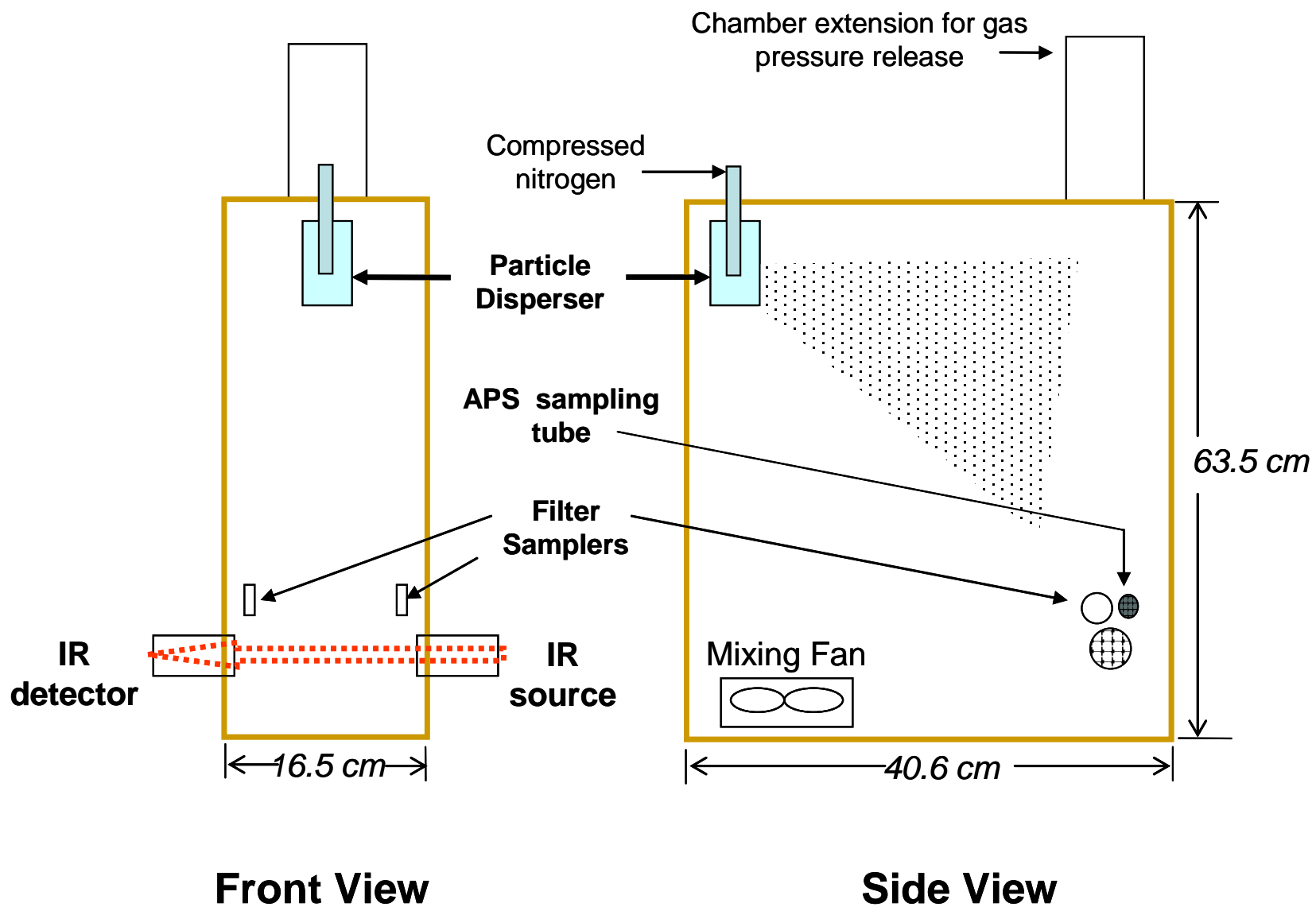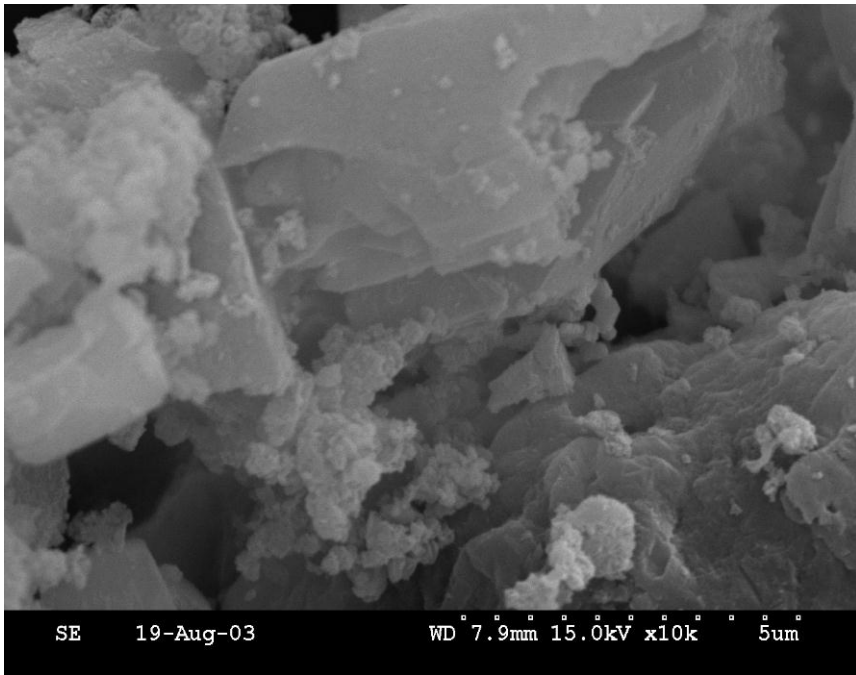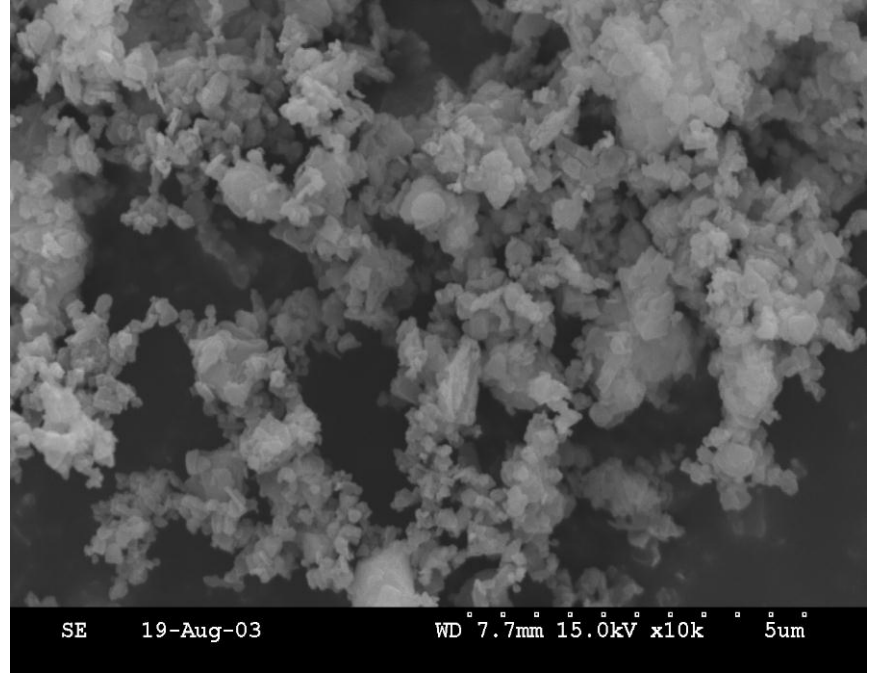
63.5 cm

Front View

Side View

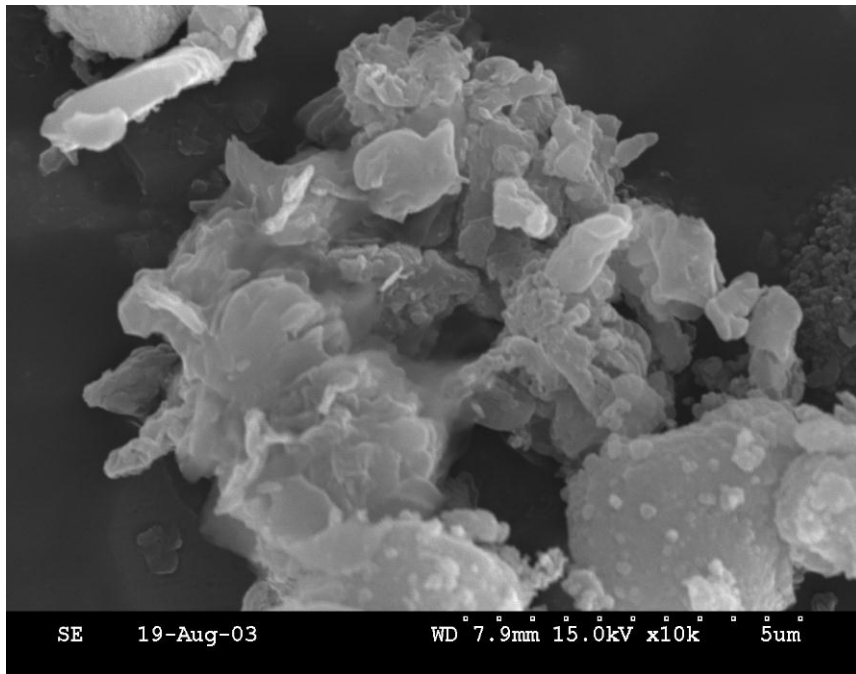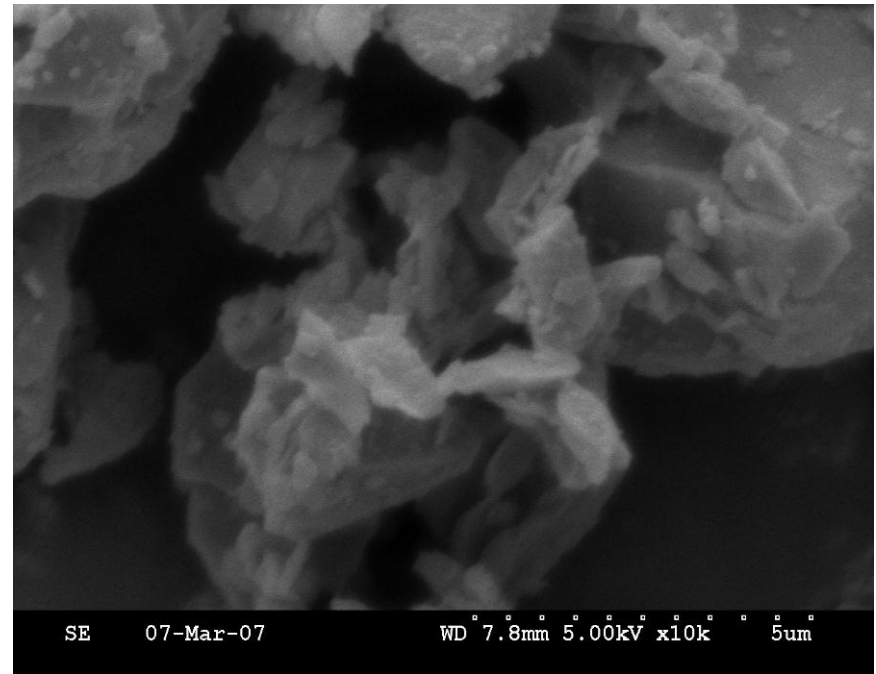Fig. 1: Schematic diagram of the experimental chamber showing the instruments (not drawn to scale).

(a)   (b)

Fig. 2: Scanning electron microscope images of the nanostructured metal oxide particles: (a) NanoActive® MgO plus and (b) NanoActive® MgO.
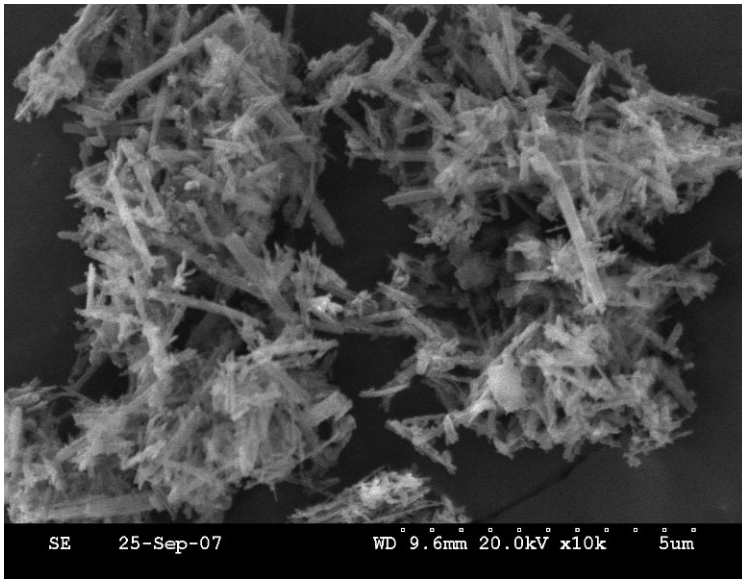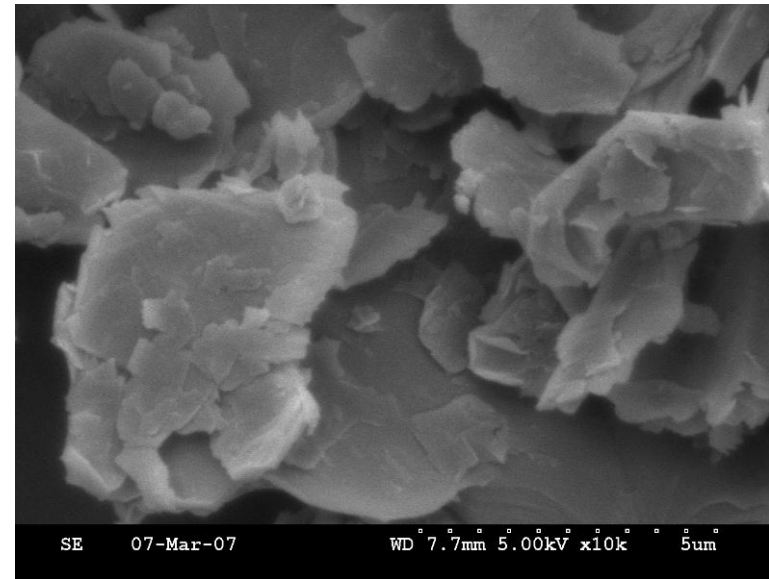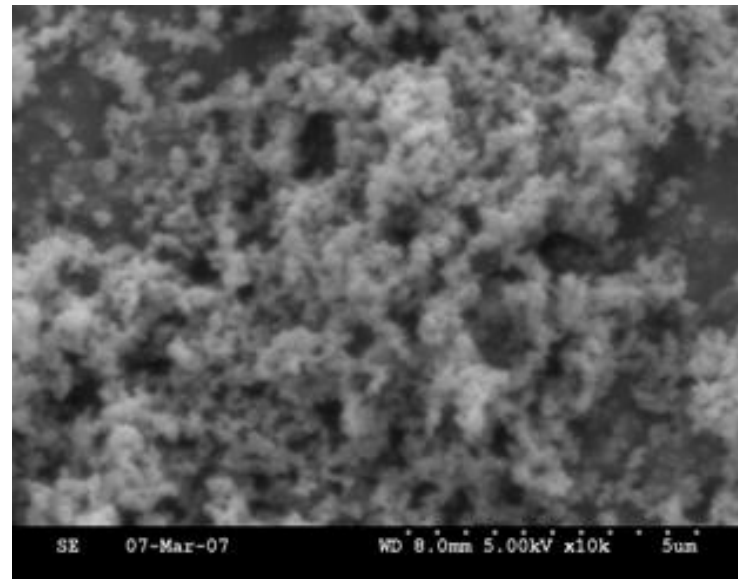
| (a) | (b) |

Fig. 3: Scanning electron microscope images of the conventional particles: (a) $NaHCO_3$ and (b) ISO fine test dust.

(a)

(b)

(c)

Fig. 4: Scanning electron microscope images of the reference particles: (a) brass flakes, (b) graphite flakes and (c) carbon black.
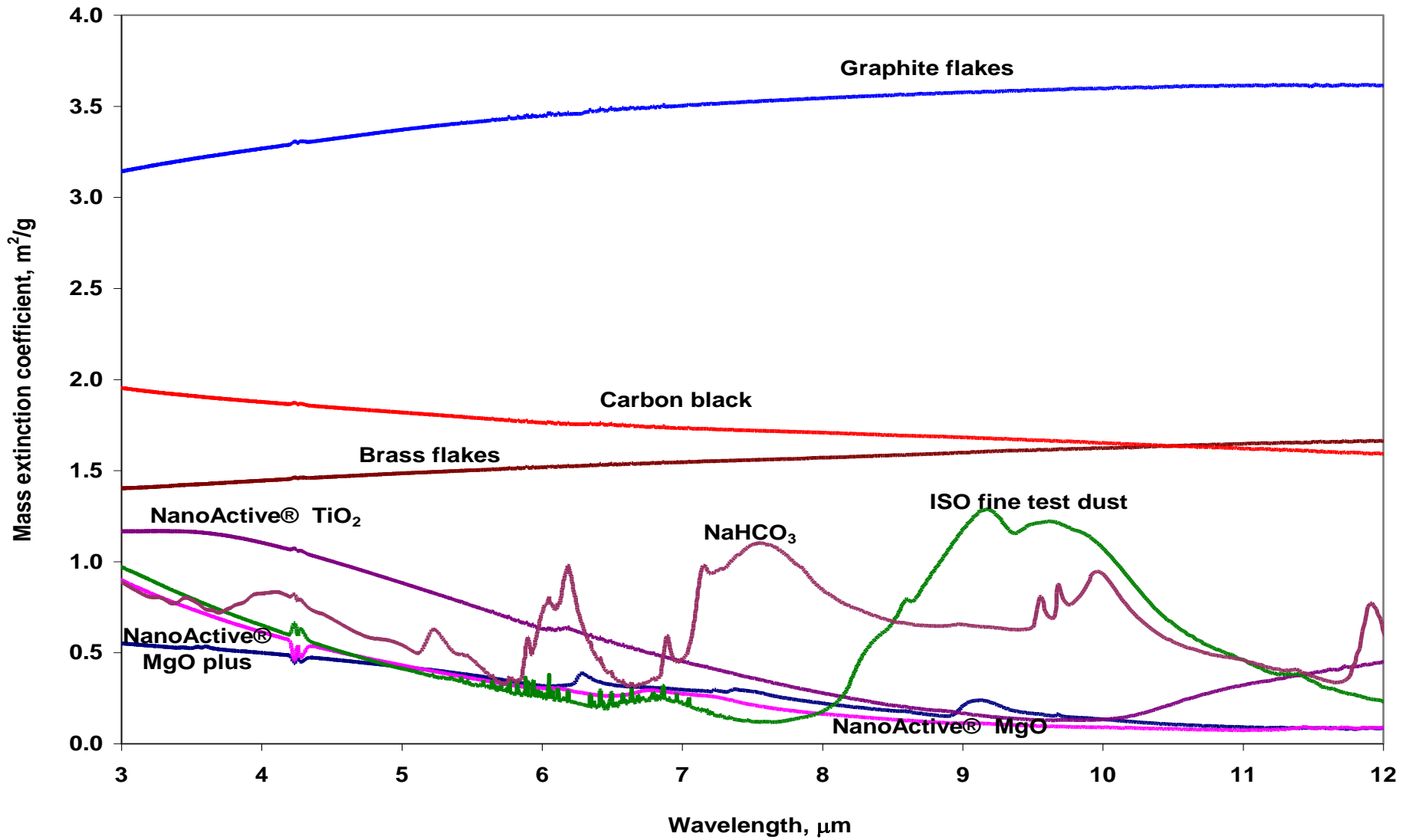
Fig. 5: Mass extinction coefficients of the particles. Each spectrum represents the mean of three replicate
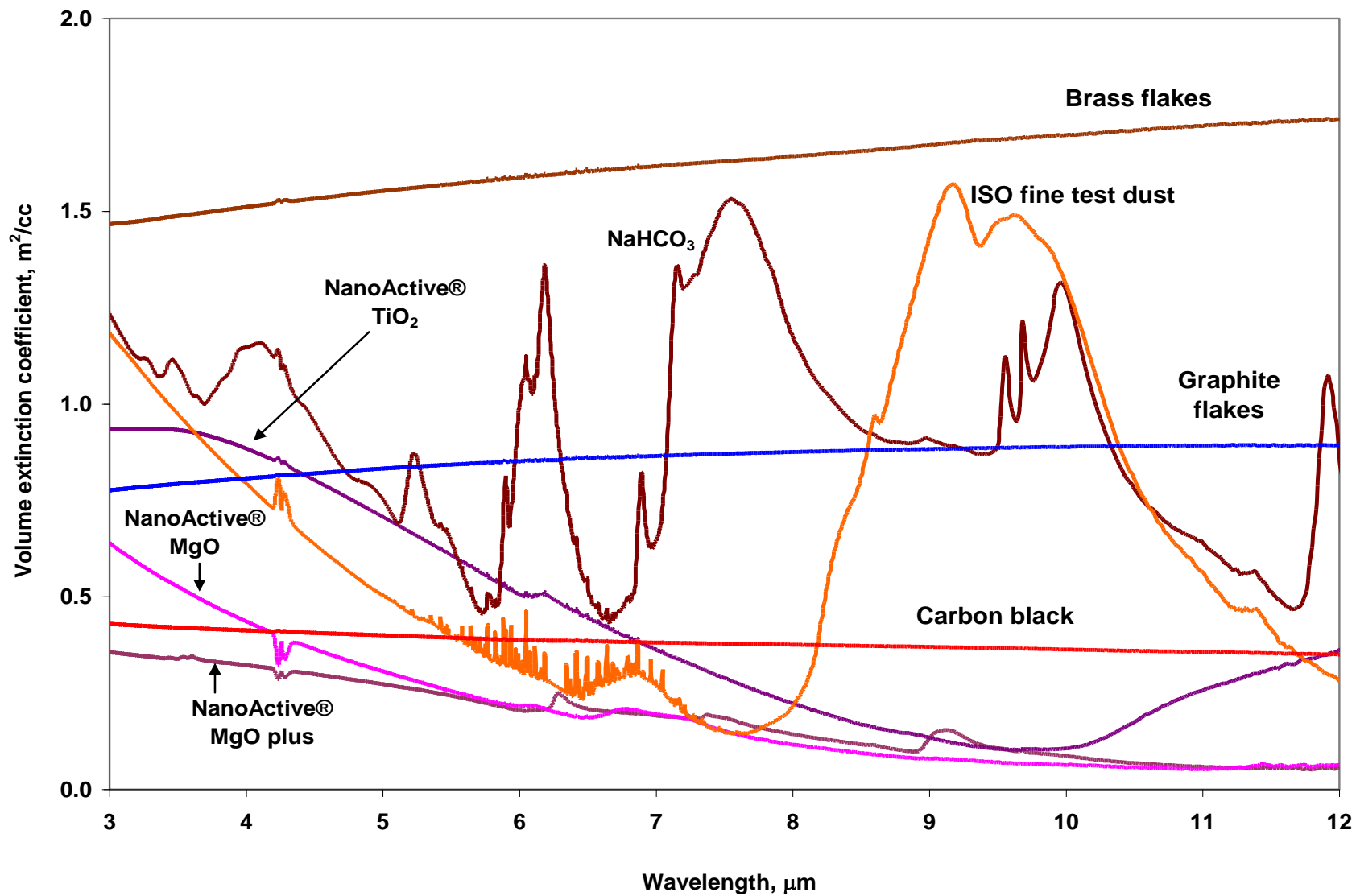
Fig. 6: Volume extinction coefficients of the different particles. Each spectrum represents the mean of three replicates.
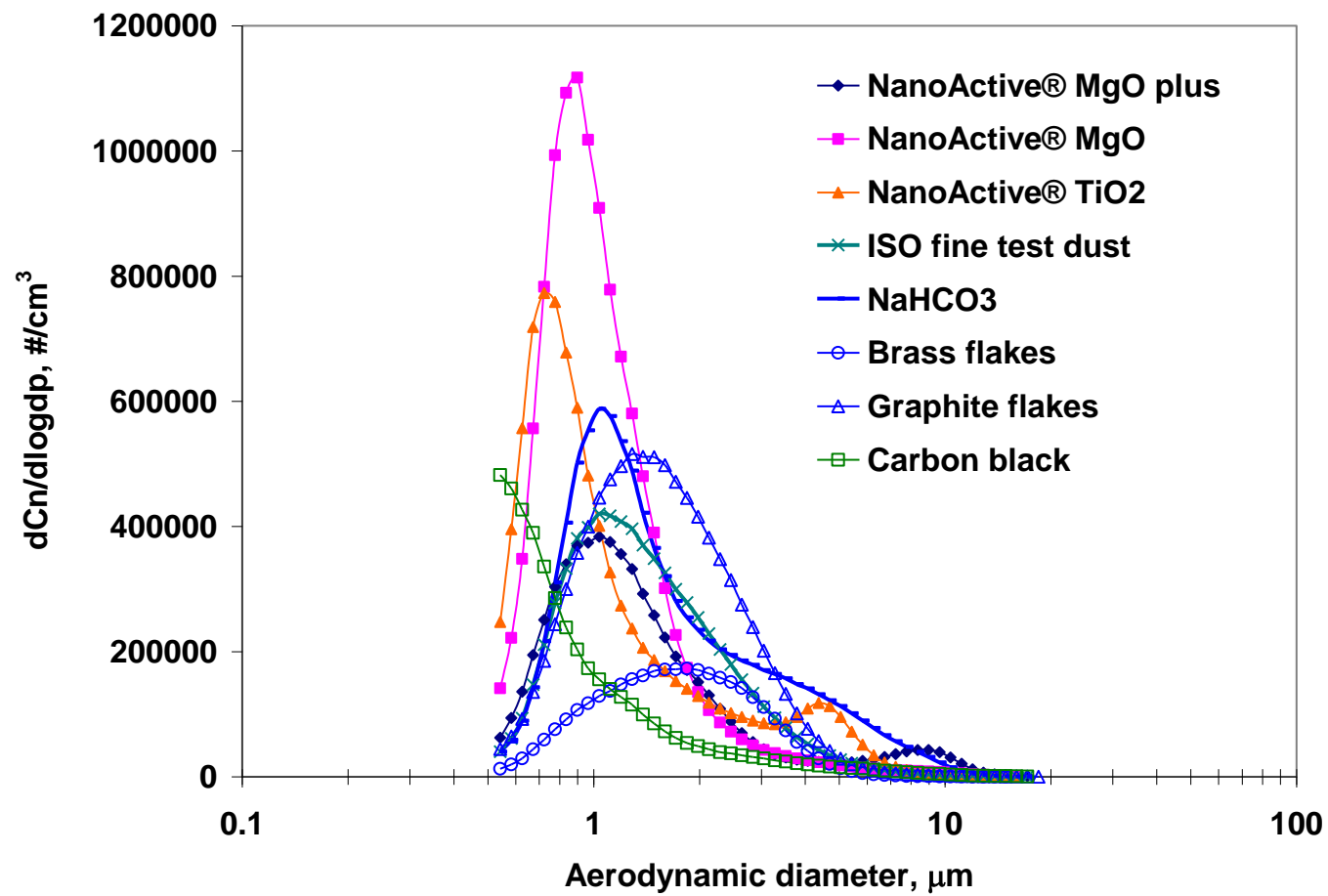
Fig. 7: Particle size distribution of the particles at time 1 min after dispersion. Each curve represents the mean of three replicates, except for the curves of the nanorods, which represent two replicates.